

BULGE-DRIVEN FUELING OF SEED BLACK HOLES

KWANGHO PARK¹, MASSIMO RICOTTI², PRIYAMVADA NATARAJAN³, TAMARA BOGDANOVIĆ¹, AND JOHN H. WISE¹

¹Center for Relativistic Astrophysics, School of Physics, Georgia Institute of Technology, Atlanta, GA 30332, USA;
kwangho.park@physics.gatech.edu

²Department of Astronomy, University of Maryland, College Park, MD 20740, USA and

³Department of Astronomy, Yale University, New Haven, CT 06520, USA

Draft version December 14, 2015

ABSTRACT

We examine radiation-regulated accretion onto intermediate-mass and massive black holes (BHs) embedded in a bulge component. Using spherically symmetric one-dimensional radiation-hydrodynamics simulations, we track the growth of BHs accreting from a cold, neutral gas reservoir with temperature $T_\infty = 10^4$ K. We find that the accretion rate of BHs embedded in bulges is proportional to $r_{\text{B,eff}}/r_{\text{B}}$, where $r_{\text{B,eff}}$ is the increased effective Bondi radius that includes the gravitational potential of the bulge, and r_{B} is the Bondi radius of the BH. The radiative feedback from the BH suppresses the cold accretion rate to ~ 1 percent of the Bondi rate when a bulge is not considered. However, we find that the BH fueling rate increases rapidly when the bulge mass M_{bulge} is greater than the critical value of $\sim 10^6 M_\odot$ and is proportional to M_{bulge} . Since the critical bulge mass is independent of the central BH mass, the growth rate of BHs with masses $M_{\text{BH}} = 10^2, 10^4$, and $10^6 M_\odot$ exhibits distinct dependencies on the bulge-to-BH mass ratio. Our results imply that light seed BHs ($\lesssim 10^2 M_\odot$) which might be the remnants of the Pop III stars, cannot grow through accretion coevally with the early assembly of the bulge of the host galaxies until the bulge reaches the critical mass. However, massive BH seeds ($\gtrsim 10^5 M_\odot$) that may form via direct collapse, are more likely to be embedded in a supercritical bulge and thus can grow efficiently coupling to the host galaxies and driving the early evolution of the $M_{\text{BH}} - \sigma$ relationship.

Subject headings: accretion, accretion disks – black hole physics – (cosmology:) early universe – galaxies: bulges – hydrodynamics – radiative transfer

1. INTRODUCTION

The discovery of the brightest high redshift quasars in the universe that are powered by 10^8 – $10^9 M_\odot$ black holes (BHs) (Fan et al. 2001, 2003; Willott et al. 2003, 2010; Fan et al. 2006; Mortlock et al. 2011) poses a challenge for models of black hole formation. How and when the initial seed black holes form and their subsequent growth history to supermassive BHs (SMBHs) at the centers of galaxies is an open problem. Recent observations of individual objects like the 13 billion M_\odot BH in the quasar detected at $z = 6.3$ (Wu et al. 2015) makes the situation even more challenging to explain. Given the nature of hierarchical build-up of structure in a LCDM universe from initial density fluctuations, we can explain a handful of extreme objects as outliers whose origin can be associated with high- σ peaks in the density field with peculiar and unusual growth histories (Natarajan & Treister 2009). However, the discovery of populations of bright quasars at progressively earlier epochs in the universe suggests that a physical explanation is required, one that might work more generally. With the growing number of discovered bright quasars at $z > 6$, it is clear that we need a theoretical model that can produce the progenitor seeds. The traditional explanation was that the initial BH seeds are the remnants of the first stars. Such scenarios for the formation of the seed BHs have suggested that intermediate-mass BHs (IMBHs) with $M_{\text{BH}} \sim 10^2 M_\odot$ may have formed out of pristine gas as Population III star remnants in the early universe (Bromm et al. 1999; Abel et al. 2000; Madau & Rees 2001) or more massive IMBHs with $M_{\text{BH}} \sim 10^4$ – $10^5 M_\odot$ from direct collapse of primordial gas (Carr et al. 1984; Haehnelt et al. 1998; Fryer et al. 2001; Begelman et al. 2006; Johnson et al. 2012; Choi

et al. 2013; Yue et al. 2014; Aykutaalp et al. 2014; Inayoshi et al. 2015b) prior to any other structure formation. Alternatively, gravitationally unstable pre-galactic disks can give rise to IMBH formation when the gas is only mildly metal-enhanced (Lodato & Natarajan 2006; Omukai et al. 2008). Or a primordial star cluster may form in the halo and this crowded environment at the core can lead to the formation of an IMBH up to $\sim 10^5 M_\odot$ (Devecchi & Volonteri 2009; Davies et al. 2011; Katz et al. 2015) or to SMBH in high redshift galaxy mergers (Mayer et al. 2015).

Thus, the growth rate of IMBHs in the range 10^2 – $10^5 M_\odot$ is essential to understand the formation and growth history of seed BHs (Madau & Rees 2001; Volonteri et al. 2003; Yoo & Miralda-Escudé 2004; Volonteri & Rees 2005; Alvarez et al. 2009; Natarajan 2011; Jeon et al. 2012). Furthermore, radiative feedback from an early population of accreting BHs can significantly impact the intergalactic medium (Mack et al. 2007; Ricotti 2009), and the associated luminosities and spectra provide a potential observational signature of a high-redshift IMBH population. Studies thus far have also provided clues to the origin of ultraluminous X-ray sources (Krolik 2004; Ricotti & Ostriker 2004; Strohmayer & Mushotzky 2009), the BHs at the centers of dwarf galaxies (Greene & Ho 2004; Reines et al. 2011, 2013; Baldassare et al. 2015), and potential IMBHs at the centers of globular clusters (e.g., Miller et al. 2014; MacLeod et al. 2015).

Standard accretion theory has difficulty in explaining the rapid growth from the proposed seed BH masses to the masses powering the observed bright quasars at high redshift (see Natarajan 2011; Volonteri 2012, for a review). A brief period of super-Eddington accretion is often invoked to jump-start BH growth for light seeds. To compute the accretion

rate onto BHs, typically the Bondi accretion model (Bondi & Hoyle 1944; Bondi 1952) is applied to estimate the gas mass accreted from the surrounding medium. Feedback from this accreting source also needs to be taken into account to estimate realistic accretion rate, and the resultant luminosity of the BH. The radiative feedback due to UV and X-ray photons from the BH forms a hot bubble of gas in the vicinity regulating gas supply from large scales not only for BHs at rest (Park & Ricotti 2011, 2012) but also for BHs in motion relative to the gas (Park & Ricotti 2013). These earlier studies found that the accretion rate drops dramatically to ~ 1 percent of the classical Bondi rate and becomes oscillatory as the ensuing feedback self-regulates the accretion flow. This is due to the fact that the gas supply into the Strömgen sphere is regulated on the scale of ionization front which is much larger than the Bondi radius. The hydrodynamic structure of the Strömgen sphere changes constantly due to this self-regulation mechanism. However, it is pressure equilibrium across the ionization front that holds the key to understanding this suppression of the accretion rate. This more physically realistic treatment, resulting in extremely low accretion rates, makes it even more challenging to explain the rapid growth of the seed BH to a few billion M_{\odot} at high redshift when the universe was less than 1 Gyr old. Our current understanding of the initial seed BH formation makes it difficult to explain the 4–7 orders of magnitude growth within that short timescale.

Locally we find that the masses of central BHs in galaxies are tightly correlated to properties of the bulge component. A correlation between BH mass and bulge velocity dispersion - the $M_{\text{BH}} - \sigma$ relation appears to hold over many decades in BH mass (Magorrian et al. 1998; Ferrarese & Merritt 2000; Tremaine et al. 2002). Observations thus reveal that BH properties are closely related to several properties of their host galaxies. Several models have been proposed to explain the driving cause for this correlation via energy or momentum-driven feedback from the central BHs. In these models, the feedback acts as a thermostat regulating BH growth rate and the star formation rate of the host galaxy (Silk & Rees 1998; King 2003; Murray et al. 2005; Springel et al. 2005; Ostriker et al. 2010).

An alternative explanation may be that the host galaxies drive the central BH masses by regulating gas supply required for their growth. In this event, it is important to understand how the BHs respond to the gas supply since the feedback-regulated accretion is the key for BH growth. The associated feedback eventually affects the properties of the host galaxies as a result. It is clear that we need to understand the interplay of the entire growth cycle of BHs and their host galaxies.

In this paper, we focus on the role played by the properties of the bulge in modulating the accretion rate onto the BH. As noted above, within the idealized Bondi accretion regime, BH growth is highly suppressed by radiative feedback, therefore it is necessary to explore other physical scenarios that can potentially boost the accretion rate. Note that the physical scale of the Bondi radius of a BH is many orders of magnitude smaller than typical galactic scales, being ~ 1 pc for $M_{\text{BH}} = 10^4 M_{\odot}$ and $T = 10^4$ K gas while the average Strömgen radius is ~ 10 pc (Park & Ricotti 2011, 2012). This implies that BHs can therefore only accrete gas from within the compact region - accretion radius - that is heated by the radiation emitted by the BH. The idealized Bondi problem setup assumes that the gravitational potential is determined only by the BH. Here, we examine the role of the other components that contribute to the gravitational potential near the

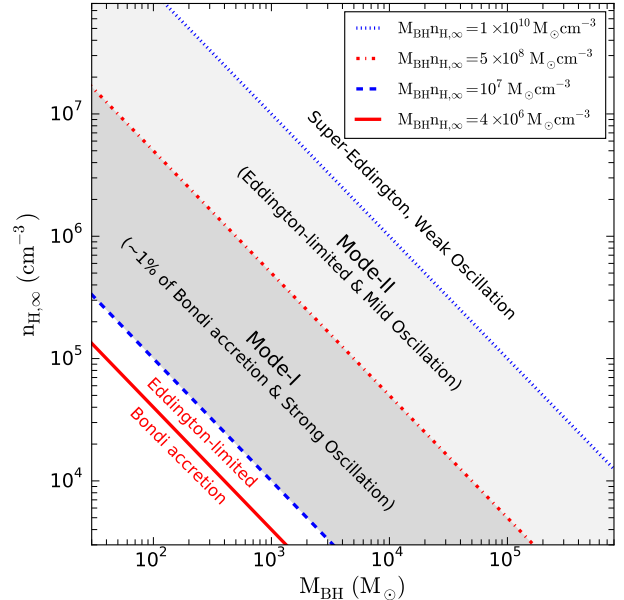


FIG. 1.— Sketch of BH accretion regimes as a function of BH mass M_{BH} and gas density $n_{\text{H},\infty}$. Solid line shows the *Eddington-limited Bondi* recipe where Eddington-limited (above the line) or Bondi accretion (below) rates are applied for a given M_{BH} and $n_{\text{H},\infty}$ for $\eta = 0.1$ and $T_{\infty} = 10^4$ K. Two distinct regimes of Mode-I and Mode-II accretion for a given M_{BH} and $n_{\text{H},\infty}$ are shown (Park & Ricotti 2012). With increasing M_{BH} or $n_{\text{H},\infty}$, the accretion onto the BH reaches the super-Eddington regime. The switch from Mode-II to super-Eddington regime in the top right corner is an approximate estimation from Park & Ricotti (2012).

BH such as a spheroidal stellar bulge. Seed BHs at the centers of galaxies do not gravitationally interact with the gas on the larger galactic scales although the bulge and dark matter halo may play an important role in delivering gas from large scales to the sub-pc scales near the BHs.

The main goal of this paper is to explore how the extended mass distribution around a BH alters the feeding rate of the first BHs. We investigate the fate of a range of seed BH masses ($10^2 - 10^6 M_{\odot}$), that are embedded in a neutral cold ($T_{\infty} \sim 10^4$ K) medium. Cold accretion might be more relevant to the growth of seed BHs in the early universe when the first galaxies start to build up their stellar mass. We generalize the results to accretion from a hot-ionized medium ($T_{\infty} \sim 10^6$ K) for simulations without radiation feedback. In section 2, we derive new scaling relationships for the generalized Bondi problem including an extended bulge mass profile and describe our numerical techniques. In section 3, we present the simulation results and discuss the results and implications in section 4.

2. METHODOLOGY

2.1. Eddington-limited Bondi accretion

The classical approach adopted to estimate the accretion rate of a BH is to compute the Bondi rate and apply the Eddington limit while considering the radiation from the BH. The Bondi radius is defined as $r_{\text{B}} \equiv GM_{\text{BH}}/c_{\text{s},\infty}^2$ where $c_{\text{s},\infty}$ is the sound speed of the gas. At the Bondi radius, the gravitational potential energy of gas equals the thermal energy of the gas, and thus the gas within r_{B} is accreted to the BH. The Bondi accretion rate can be expressed as a function of BH mass M_{BH} , ambient gas density ρ_{∞} , and sound speed $c_{\text{s},\infty}$ of

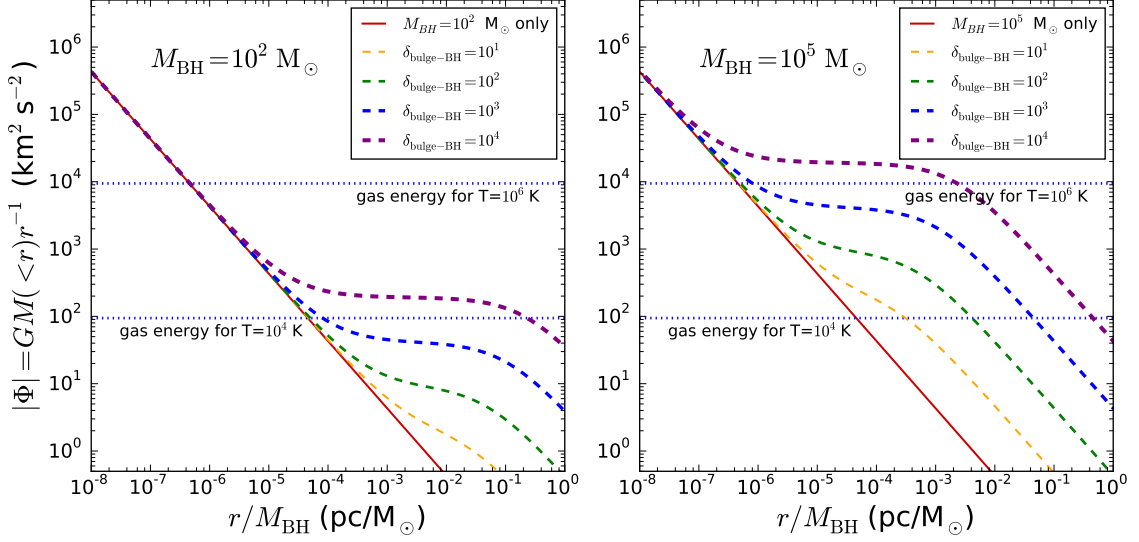


FIG. 2.— Gravitational potential energy Φ with a bulge component as a function of radius for $M_{\text{BH}} = 10^2 M_{\odot}$ (left) and $M_{\text{BH}} = 10^5 M_{\odot}$ (right). The scale radius a for a given bulge mass is adjusted so that the mass density is fixed within a . The radii are normalized by the BH mass and the gravitational constant $G = 4.3 \times 10^{-3} \text{ pc } M_{\odot}^{-1} (\text{km s}^{-1})^2$ is used for Φ . The horizontal dotted lines indicate the gas energy for $T = 10^4 \text{ K}$ and 10^6 K . The intersection of Φ and the gas energy is analogous to *Bondi radius* within which the gravitational energy dominates over the gas energy. Note that the effective Bondi radius as a function of bulge mass changes as a function of BH mass and gas temperature.

the gas as

$$\dot{M}_{\text{B}} = 4\pi\lambda_{\text{B}}\rho_{\infty} \frac{G^2 M_{\text{BH}}^2}{c_{\text{s},\infty}^3} \quad (1)$$

where λ_{B} is the dimensionless accretion rate as a function of the equation of state ($P \propto \rho^{\gamma}$). The factor λ_{B} ranges from $e^{3/2}/4$ for an isothermal gas ($\gamma = 1$) to $1/4$ for an adiabatic gas ($\gamma = 5/3$). The Eddington luminosity is defined as the maximum accretion rate for a BH with M_{BH} considering the radiation from the BH and expressed as

$$L_{\text{Edd}} = 4\pi G M_{\text{BH}} m_{\text{p}} c \sigma_{\text{T}}^{-1} \quad (2)$$

where m_{p} is the proton mass, σ_{T} is the Thompson cross section, and c is the speed of light. The regimes where the Bondi accretion or Eddington-limited accretion occur can be found by comparing \dot{M}_{B} and $L_{\text{Edd}}/(\eta c^2)$ where η is the radiative efficiency. For the case without radiative feedback from the growing BH, assuming $\eta = 0.1$ and $T_{\infty} = 10^4 \text{ K}$ the two regimes are separated by $M_{\text{BH}} n_{\text{H},\infty} = 4 \times 10^6 M_{\odot} \text{ cm}^{-3}$ shown as a solid line at the bottom left corner of Figure 1.

2.2. Radiation-regulated accretion: Mode-I and II

When the radiative feedback from the growing BH is taken into account, the accretion rate is suppressed and displays a highly oscillatory behavior (Milosavljević et al. 2009; Li 2011; Park & Ricotti 2011, 2012). Park & Ricotti (2012) find that two distinct types of oscillations are expected depending on the values of M_{BH} and $n_{\text{H},\infty}$, which are separated by a dot-dashed line shown in Figure 1. In *Mode-I* accretion, the thermal pressure gradient dominates over the gravity inside the Strömgen sphere, and bursts of accretion are driven by the collapse of neutral gas once the gas inside the Strömgen sphere is depleted. On the other hand, the oscillation of accretion rate in *Mode-II* is driven by density waves from the ionization front. The transition between Mode-I (strong) oscillation with an accretion rate of ~ 1 percent of Bondi rate to

Mode-II (mild) oscillation with Eddington-limited rate occurs approximately at

$$M_{\text{BH}} n_{\text{H},\infty}^{\text{cr}} \sim 5 \times 10^8 M_{\odot} \text{ cm}^{-3} \quad (3)$$

where $n_{\text{H},\infty}^{\text{cr}}$ is the critical density for a given BH mass M_{BH} . Note that the Eddington-limited accretion regime including radiation feedback is found at higher M_{BH} and $n_{\text{H},\infty}$ compared to the conventional *Eddington-limited Bondi accretion* criteria shown in Figure 1 as a solid red line.

The behavior of the accretion rate is expected to make another transition at extremely high densities, large values of $n_{\text{H},\infty}$ for a given M_{BH} , when the oscillatory behavior weakens and the radiative feedback is no longer able to regulate gas accretion. This *super-Eddington* or *hyper-accretion* (e.g., Ohsuga & Mineshige 2011; Jiang et al. 2014) regime occurs when the accretion far exceeds the Eddington rate. The dotted line in Figure 1 is an upper boundary for Mode-II accretion covered in Park & Ricotti (2012) assuming $\eta = 0.1$. With increasing density for a given BH mass (moving upward in Figure 1) or increasing BH mass for a fixed gas density (moving to the right in Figure 1), the accretion is expected to make a transition from the “*feedback-dominated*” to the “*feeding-dominated*” regime (e.g., Pacucci et al. 2015). Inayoshi et al. (2015a) also explore a critical accretion regime choosing a photon trapping model motivated by Begelman (1979). They derive the hyper-accretion regime using the instability of the ionization front (Park et al. 2014a) when the scale of the photo-ionized region becomes smaller the Bondi radius. Of course, physical conditions in the early universe do permit super-Eddington accretion under certain specific circumstances, as recently pointed out by Alexander & Natarajan (2014) when a light BH seed captured in a dense nuclear star cluster bounces around as it accretes.

2.3. Generalized Bondi accretion with a bulge component

We now describe the accretion onto a BH surrounded by a bulge component whose gravitational potential we now in-

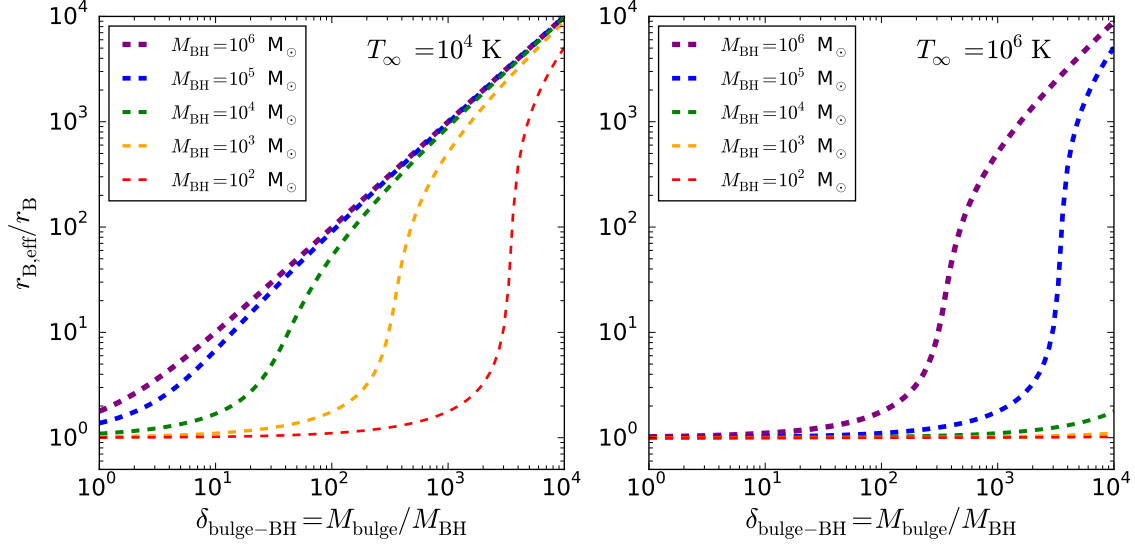


FIG. 3.— Effective Bondi radius as a function of bulge-to-BH mass ratio $\delta_{\text{bulge-BH}} = M_{\text{bulge}}/M_{\text{BH}}$ for $M_{\text{BH}} = 10^2, 10^3, 10^4, 10^5,$ and $10^6 M_{\odot}$. Left panel shows $r_{\text{B,eff}}$ for cold gas with $T_{\infty} = 10^4$ K and right panel shows $r_{\text{B,eff}}$ for hot gas with $T_{\infty} = 10^6$ K.

clude to derive an analog to Bondi accretion. To calculate the modified Bondi radius, we model the radial profile of the stellar distribution with a Hernquist (1990) profile. And the corresponding gravitational potential can be described in terms of the total bulge mass M_{bulge} and the scale length a

$$\Phi_{\text{bulge}}(r) = -\frac{GM_{\text{bulge}}}{r+a} \quad (4)$$

where the enclosed mass within the radius r is $m(r) = M_{\text{bulge}}r^2/(r+a)^2$. The mean density within the scale radius a is then obtained as

$$\bar{\rho}_*(r < a) = \frac{3m(a)}{4\pi a^3} = \frac{3M_{\text{bulge}}}{16\pi a^3}. \quad (5)$$

For a given bulge mass, we keep the same density within the scaling radius a by applying $a = a_0(M_{\text{bulge}}/M_{\odot})^{1/3}$. The Milky Way for instance has a bulge mass $M_{\text{bulge}} \sim 10^{10} M_{\odot}$ with scale radius $a_{\text{MW}} \sim 800$ pc and the DM halo mass $M_{\text{DM}} \sim 10^{12} M_{\odot}$ (Dwek et al. 1995; Widrow & Dubinski 2005; Kafle et al. 2014). The average stellar density within the scale radius for the MW is estimated to be $\sim 1 M_{\odot}\text{pc}^{-3}$. Here we use $a_0 = 0.23$ pc which corresponds to $\bar{\rho}_* \sim 5.2 M_{\odot}\text{pc}^{-3}$. The $\bar{\rho}_*$ is obviously a free parameter, however note that a_0 is not very sensitive to $\bar{\rho}_*$ since $a_0 \propto \bar{\rho}_*^{-1/3}$ for a given bulge mass.

We define the effective Bondi radius $r_{\text{B,eff}}$ as

$$\frac{GM_{\text{BH}}}{r_{\text{B,eff}}} + \frac{GM_{\text{bulge}}}{r_{\text{B,eff}} + a} \equiv c_{\infty}^2 \quad (6)$$

where the left side of the equation is the magnitude of the gravitational potential per unit mass due to the BH and bulge component, whereas the right side represents the thermal energy of the gas per unit mass. Figure 2 shows the magnitude of the combined gravitational potential Φ . The horizontal dotted lines indicate the specific thermal energy of cold gas with $T_{\infty}=10^4$ K and hot gas with $T_{\infty} = 10^6$ K more appropriate for massive halos (McKee & Ostriker 1977; Springel & Hernquist 2003; Pelupessy et al. 2007). Its intersection with Φ for

various values of $\delta_{\text{bulge-BH}} \equiv M_{\text{bulge}}/M_{\text{BH}}$ is the solution for the effective Bondi radius $r_{\text{B,eff}}$. The solution for the effective radius in turn can be obtained as

$$\frac{r_{\text{B,eff}}}{r_{\text{B}}} = 0.5 \times \left[\delta_{\text{bulge-BH}} + 1 - a' + \sqrt{(a' - 1 - \delta_{\text{bulge-BH}})^2 + 4a'} \right] \quad (7)$$

where the radii are normalized by the Bondi radius as $a' \equiv a/r_{\text{B}}$ and $\delta_{\text{bulge-BH}}$ is defined as the bulge-to-BH mass ratio $M_{\text{bulge}}/M_{\text{BH}}$.

Figure 3 shows the effective Bondi radius normalized by the Bondi radius $r_{\text{B,eff}}/r_{\text{B}}$ for different BH masses $10^2, 10^3, 10^4, 10^5,$ and $10^6 M_{\odot}$. For cold gas with $T_{\infty} = 10^4$ K (left panel), the $r_{\text{B,eff}}/r_{\text{B}}$ for light BHs with $M_{\text{BH}} = 10^2 M_{\odot}$ does not increase significantly for $\delta_{\text{bulge-BH}} \lesssim 10^3$ whereas $r_{\text{B,eff}}/r_{\text{B}}$ for the massive IMBH with $M_{\text{BH}} \gtrsim 10^5 M_{\odot}$ monotonically increases with $\delta_{\text{bulge-BH}}$. This implies that the accretion onto various BH masses is affected differently with the same $\delta_{\text{bulge-BH}}$ since the gas within $r_{\text{B,eff}}$ is pulled in to the BH by the enhanced gravitational potential.

2.4. Critical Bulge Mass

From Equation (7), as illustrated in Figure 3, it is evident that there exists a critical bulge mass above which $r_{\text{B,eff}}/r_{\text{B}}$ transitions from unity to being linearly proportional $\delta_{\text{bulge-BH}}$: thus from the BH Bondi radius to what we now term the ‘‘bulge’’ Bondi radius.

The critical value of the bulge mass can be derived from Equation (7) noting that $a' \equiv a/r_{\text{B}} = C\delta_{\text{bulge-BH}}$, where $C = [a_0/r_{\text{B}}(1 M_{\odot})](M_{\text{bulge}}/1 M_{\odot})^{-2/3}$, and the transition between $r_{\text{B,eff}}/r_{\text{B}}$ of unity to $\delta_{\text{bulge-BH}}$ happens roughly when $C = 1$, i.e., when

$$a = r_{\text{B}}\delta_{\text{bulge-BH}} = \frac{GM_{\text{bulge}}}{c_{s,\infty}^2}. \quad (8)$$

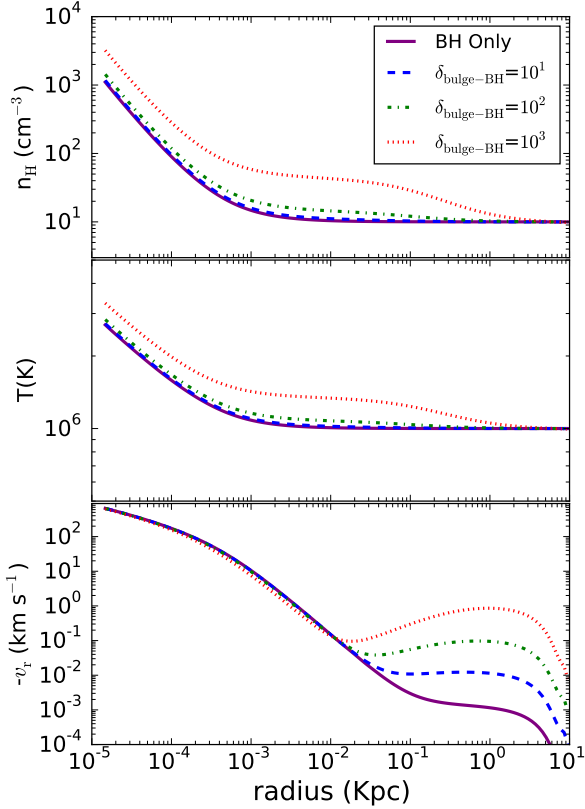


FIG. 4.— Density (top), temperature (middle), and radial velocity (bottom) as a function of radius for simulations (M6N1T6NR) without radiative feedback for $M_{\text{BH}} = 10^6 M_{\odot}$, $n_{\text{H},\infty} = 10 \text{ cm}^{-3}$, $T_{\infty} = 10^6 \text{ K}$, and $\gamma = 1.2$. All the profiles shown are the steady states for $\delta_{\text{bulge-BH}} = 0$ (solid), 10^1 (dashed), 10^2 (dot-dashed), and 10^3 (dotted). Inflow velocity at large radius increases as a function of $\delta_{\text{bulge-BH}}$, however the velocity is at small radius is determined by the gravitational potential by the BH. The density and temperature profiles do not change significantly until $\delta_{\text{bulge-BH}} \lesssim 10^2$, but shows an enhancement at $\delta_{\text{bulge-BH}} = 10^3$ which is consistent with the behavior of $r_{\text{B,eff}}$ for $T_{\infty} = 10^6 \text{ K}$ in Figure 3.

Setting $C = 1$, we derive the critical bulge mass at which the gas accretion rate onto the BH transitions from the case of an isolated BH to being force-fed by the bulge:

$$M_{\text{bulge,crit}} \sim 4 \times 10^5 M_{\odot} \left(\frac{T_{\infty}}{10^4 \text{ K}} \right)^{3/2} \left(\frac{\bar{\rho}_*}{5.2 M_{\odot} \text{pc}^{-3}} \right)^{-1/2} \quad (9)$$

Figure 3 shows that the value of $\delta_{\text{crit}} \equiv M_{\text{bulge,crit}}/M_{\text{BH}}$ above which the $r_{\text{B,eff}}$ shows a linear relationship with $\delta_{\text{bulge-BH}}$ is $\delta_{\text{crit}} \sim 4000$ for $10^2 M_{\odot}$ BHs, $\delta_{\text{crit}} \sim 400$ for $10^3 M_{\odot}$ BHs, and $\delta_{\text{crit}} \sim 40$ for $10^4 M_{\odot}$ BHs. This is indeed what was expected if there is a critical bulge mass $M_{\text{bulge,crit}} \sim 4 \times 10^5 M_{\odot}$ as given by Equation (9) for $T_{\infty} = 10^4 \text{ K}$. For hot gas with $T_{\infty} = 10^6 \text{ K}$ which is more typical of the hot virialized gas in massive ellipticals or the hot ionized medium in the ISM, $r_{\text{B,eff}}/r_{\text{B}}$ for various BH mass is shown in the right panel of Figure 3. Note that the $r_{\text{B,eff}}/r_{\text{B}}$ for a given BH mass for hot gas with T_{hot} matches the case for lower BH mass $M_{\text{BH}}(T_{\text{cold}}/T_{\text{hot}})^{3/2}$, as in Equation (9). For example, the value of $r_{\text{B,eff}}$ for $M_{\text{BH}} = 10^6 M_{\odot}$

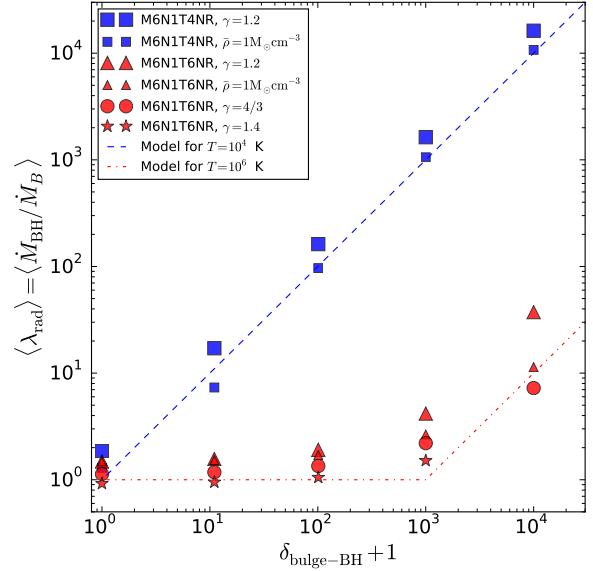


FIG. 5.— Average accretion rates normalized by Bondi rate for simulations M6N1T4NR for cold gas ($T_{\infty} = 10^4 \text{ K}$) shown as squares and M6N1T6NR for hot gas ($T_{\infty} = 10^6 \text{ K}$) shown as triangles ($\gamma = 1.2$), circles ($\gamma = 4/3$), and stars ($\gamma = 1.4$). Average accretion rate increases as a function of $\delta_{\text{bulge-BH}}$ when $\delta_{\text{bulge-BH}} \gtrsim \delta_{\text{crit}}$. Note that $\delta_{\text{crit}} \sim 1$ for cold gas while $\delta_{\text{crit}} \sim 10^3$ for hot gas ($T_{\infty} = 10^6 \text{ K}$).

and $T_{\infty} = 10^6 \text{ K}$ matches the one for $M_{\text{BH}} = 10^3 M_{\odot}$ and $T_{\infty} = 10^4 \text{ K}$.

2.5. 1D Radiation-hydrodynamic Simulations

Radiation-hydrodynamic simulations are a useful tool to investigate the complex interplay between accretion flows and radiative feedback in the modified Bondi problem with a bulge component. In this section, we describe the numerical procedures used in our study. We run a set of 1D radiation-hydrodynamics simulations using ZEUS-MP (Stone & Norman 1992; Hayes et al. 2006) with a radiative transfer equation solver (Ricotti et al. 2001). We use a spherical coordinate system with a BH centered at $r = 0$ applying an operator-splitting method between hydrodynamic and radiative transfer calculations. At the minimum radius, we use the mass flux (\dot{M}_{BH}) to define the BH luminosity as $L_{\text{bh}} = \eta \dot{M}_{\text{BH}} c^2$. We apply a power-law spectrum $F_{\nu} \propto \nu^{-\alpha}$ where α is the spectral index for BH radiation in the energy range from 13.6 eV to 100 keV and $\alpha = 1.5$ is used. Our radiative transfer subroutine calculates photo-heating, photo-ionization, radiation pressure, and gas cooling. Compton heating is neglected in this study since the effect is not significant when the incident spectrum is soft in high accretion rate regime (Park et al. 2014b).

The basic setup of the current work is similar to the previous works (Park & Ricotti 2011, 2012), but we add a bulge component to the gravitational potential (see section 2.3). Different pairs of values for M_{BH} and $n_{\text{H},\infty}$ are selected, but we keep $M_{\text{BH}} n_{\text{H},\infty} = 10^7 M_{\odot} \text{cm}^{-3}$, so that we can separate the effect of the bulge on the growth history of different BH seed masses. Simulations with the same value of $M_{\text{BH}} n_{\text{H},\infty}$ show qualitatively similar results in terms of the accretion rate normalized by the Bondi rate and the period of oscillation when normalized by M_{BH} . Also, our assumption ensures

TABLE 1
SIMULATION PARAMETERS

ID	M_{BH} (M_{\odot})	$n_{\text{H},\infty}$ (cm^{-3})	T_{∞} (K)	γ	Rad Feedback	$\delta_{\text{bulge-BH}}$
M6N1T4NR	10^6	10^1	10^4	1.2	No	$0, 10^1, 10^2, 10^3, 10^4$
M6N1T6NR	10^6	10^1	10^6	1.2, 4/3, 1.4	No	$0, 10^1, 10^2, 10^3, 10^4$
M2N5	10^2	10^5	10^4	5/3	Yes	$0, 3, 10, 30, 10^2, 3 \times 10^2, 10^3, 3 \times 10^3, 10^4$
M4N3	10^4	10^3	10^4	5/3	Yes	$0, 3, 10, 30, 10^2, 3 \times 10^2, 10^3, 3 \times 10^3$
M6N1	10^6	10^1	10^4	5/3	Yes	$0, 3, 10, 30, 10^2, 3 \times 10^2, 10^3$

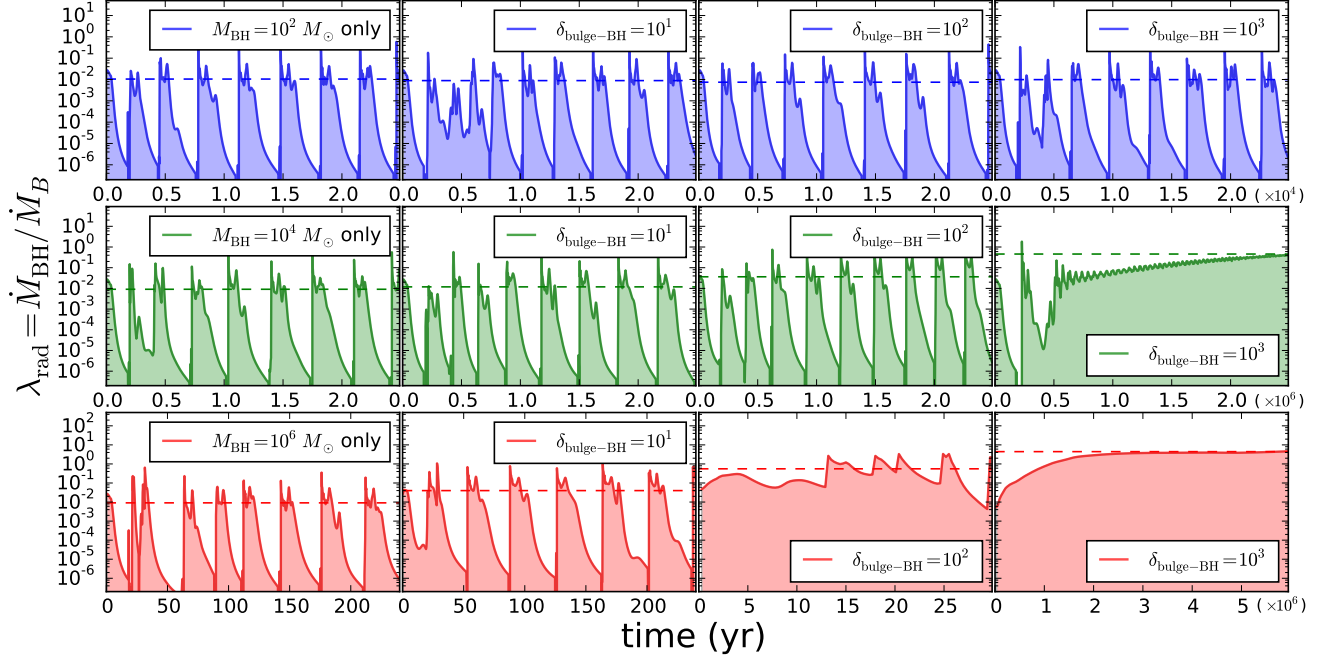


FIG. 6.— Accretion rates as a function of time for various bulge-to-BH mass ratios $\delta_{\text{bulge-BH}}$. Dashed lines show the mean accretion rates if the accretion is oscillatory or asymptotic values otherwise. Top panels show the simulations for M2N5, middle panels show M4N3, and bottom panels show M6N1. For various $\delta_{\text{bulge-BH}}$, M2N5 does not show significant change as a function of $\delta_{\text{bulge-BH}}$. For M4N3, due to the increased effective Bondi radius $r_{\text{B,eff}}$ the accretion rate increases as a function of $\delta_{\text{bulge-BH}}$ when $\delta_{\text{bulge-BH}} \gtrsim 10^2$. For M6N1, the accretion rate increases when $\delta_{\text{bulge-BH}} \gtrsim 1$.

that the growth timescale of BHs accreting at the Bondi rate, $M_{\text{BH}}/\dot{M}_{\text{B}} \propto M_{\text{BH}}n_{\text{H},\infty}$, is kept constant in all simulations with different BH masses. Simulation parameters are listed in Table 1. M2N5, M4N3, and M6N1 are simulations with radiative feedback for BHs with 10^2 , 10^4 , and $10^6 M_{\odot}$ and keeping the same $M_{\text{BH}}n_{\text{H},\infty}$. M6N1T4NR and M6N1T6NR are simulations without radiative feedback for $M_{\text{BH}} = 10^6 M_{\odot}$, 10 cm^{-3} , and $T_{\infty} = 10^4 \text{ K}$ and 10^6 K , respectively.

3. RESULTS

3.1. Generalized Bondi Accretion without Radiative Feedback

Figure 4 shows the density (top), temperature (middle), and radial velocity of the gas (bottom) as a function of radius for simulations M6N1T6NR without radiative feedback with $\gamma = 1.2$ and $M_{\text{BH}} = 10^6 M_{\odot}$ accreting from a gas with temperature $T = 10^6 \text{ K}$. The radial profiles have reached steady state accretion and the different colored lines (see legend) refer to different bulge masses: $\delta_{\text{bulge-BH}} = 10^1, 10^2$, and 10^3 (i.e., $M_{\text{bulge}} = 10^7, 10^8$, and $10^9 M_{\odot}$). The density and temperature profiles do not change until $M_{\text{bulge}} \gtrsim 10^8$, but

display an enhancement at $M_{\text{bulge}} = 10^9$, that is consistent with $M_{\text{bulge,crit}}$ in Equation (9) for $T_{\infty} = 10^6 \text{ K}$ and with Figure 3.

The change of accretion rate observed when $M_{\text{bulge}} > M_{\text{bulge,crit}}$ for the simulation without radiative feedback appears to be dominated by an increase in the density produced by the presence of the bulge component. While the velocity near the BH is not altered as shown in Figure 4. The central temperature rises mildly, reducing by the same magnitude of the Bondi radius. Therefore the dominant effect that causes an increase in the accretion rate is the enhanced density near the Bondi radius of the BH.

We find that the accretion rate is \dot{M}_{B} if $M_{\text{bulge}} \leq M_{\text{bulge,crit}}$ and increases as

$$\dot{M}_{\text{BH}} \sim \dot{M}_{\text{B}} \frac{M_{\text{bulge}}}{M_{\text{bulge,crit}}}, \quad (10)$$

for $M_{\text{bulge}} > M_{\text{bulge,crit}}$. Figure 5 shows accretion rates as a function of the bulge mass for a set of simulations of $10^6 M_{\odot}$ BHs without radiative feedback but with different values for γ , the temperature of the gas, and density of the bulge (see simulations M6N1T4NR and M6N1T6NR in Table 1). We

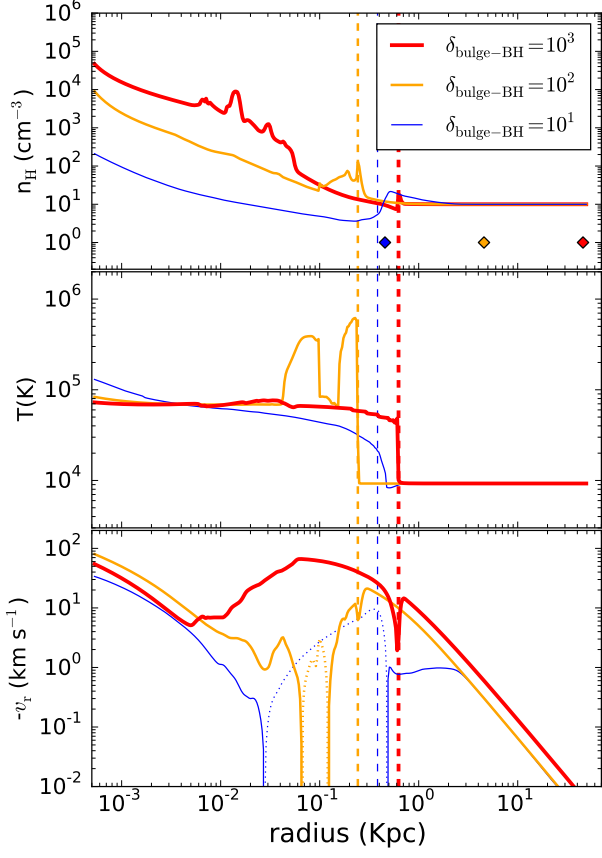


FIG. 7.— Time-averaged hydrogen number density (top), temperature (middle), and radial velocity (bottom) profiles as a function of radius for $M_{\text{BH}} = 10^6 M_{\odot}$ and $n_{\text{H},\infty} = 10 \text{ cm}^{-3}$ simulations. For v_r , solid line is inflow while outflow is shown as dotted. Different colors show the runs with $\delta_{\text{bulge-BH}} = 10^1, 10^2$, and 10^3 , respectively. Vertical dashed lines show the time-averaged mean size of the Strömgren sphere for each simulation. Diamonds in the top panel from left to right indicate $r_{\text{B,eff}}$ for simulations with $\delta_{\text{bulge-BH}} = 10^1, 10^2$, and 10^3 , respectively. Note that $r_{\text{B,eff}}$ for $\delta_{\text{bulge-BH}} = 10^1$ is comparable to the mean size of the Strömgren sphere. As the $\delta_{\text{bulge-BH}}$ increases, the $r_{\text{B,eff}}$ becomes larger than the Strömgren radius.

find that Equation (9) and (10) accurately describe the accretion rate from the simulations: the accretion rate remains constant when $M_{\text{bulge}} \leq M_{\text{bulge,crit}}$ ($\delta_{\text{bulge-BH}} \leq \delta_{\text{crit}}$) while it increases linearly with M_{bulge} for $M_{\text{bulge}} > M_{\text{bulge,crit}}$ ($\delta_{\text{bulge-BH}} > \delta_{\text{crit}}$). As mentioned in section 2.3, simulations with a lower stellar density $\bar{\rho}_* \sim 1 M_{\odot} \text{pc}^{-3}$ (shown as small squares and triangles) do not show a significant difference from simulations with $\bar{\rho}_* \sim 5.2 M_{\odot} \text{pc}^{-3}$ since the bulge scale length a is not very sensitive to $\bar{\rho}_*$.

3.2. Generalized Bondi Accretion with Radiative Feedback

Figure 6 shows accretion rates as a function of time for $\delta_{\text{bulge-BH}} = 0, 10^1, 10^2$, and 10^3 for simulations M2N5 ($M_{\text{BH}} = 100 M_{\odot}$, top panels), M4N3 ($M_{\text{BH}} = 10^4 M_{\odot}$, middle panels), and M6N1 ($M_{\text{BH}} = 10^6 M_{\odot}$, bottom panels). The mean accretion rates are shown as dashed lines in each panel. These 3 sets of simulations share the same value of $M_{\text{BH}} n_{\text{H},\infty}$ and $T_{\infty} = 10^4 \text{ K}$, thus have the same growth timescale and the same oscillatory behavior in absence of the bulge component (first columns). However, including the effect of various bulge masses the accretion be-

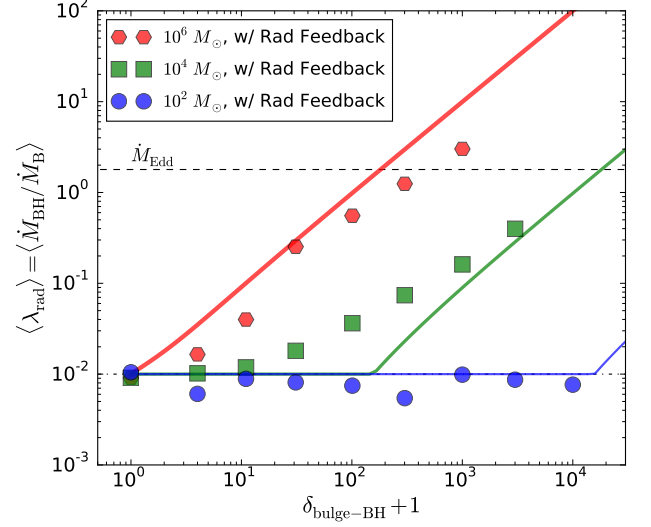


FIG. 8.— Average accretion rates normalized by Bondi rate for simulations M2N5 (circles), M4N3 (squares), and M6N1 (hexagons). Average accretion rate increases as a function of $\delta_{\text{bulge-BH}}$ when $\delta_{\text{bulge-BH}} \gtrsim \delta_{\text{crit}}$ while accretion rate remains the same when $\delta_{\text{bulge-BH}} \lesssim \delta_{\text{crit}}$ for all simulations. Since δ_{crit} is small (~ 1) for M6N1, the average accretion rate always increases with increasing bulge mass $\delta_{\text{bulge-BH}}$. On the other hand, the accretion rate does not increase as a function of $\delta_{\text{bulge-BH}}$ for M2N5 since δ_{crit} is large ($\sim 10^4$).

havior displays significant differences. For a $10^2 M_{\odot}$ BH (M2N5), the assumed $\delta_{\text{bulge-BH}}$ produces negligible effects. The accretion shows oscillatory behavior for the entire range of M_{bulge} shown here ($M_{\text{bulge}} \leq 10^5 M_{\odot}$) and the mean accretion rate does not change significantly. Therefore, the presence of a bulge with $M_{\text{bulge}} \leq 10^5 M_{\odot}$ does not alter the growth rate of light seed BHs. On the other hand, the accretion onto a $10^4 M_{\odot}$ BH shows a transition from oscillatory behavior for $M_{\text{bulge}} \lesssim 10^6 M_{\odot}$ to quasi-steady state accretion for $M_{\text{bulge}} \gtrsim 10^7 M_{\odot}$. The transition occurs at a smaller bulge-to-BH ratio $\delta_{\text{bulge-BH}} \gtrsim 10^2$ for a $10^6 M_{\odot}$ BH (M6N1), corresponding to $M_{\text{bulge}} \gtrsim 10^8 M_{\odot}$. Therefore, to zeroth order, the effect of the bulge on the mean accretion rate for the case with radiative feedback appear to be fairly similar to what we found in the case neglecting radiative feedback. However, the transition from oscillatory behavior to steady accretion happens for somewhat larger bulge masses than $M_{\text{bulge,crit}} = 10^6 M_{\odot}$ when radiative feedback is included and is mildly dependent on $\delta_{\text{bulge-BH}}$. By increasing the bulge mass, the accretion onto BHs transitions from a duty cycle of $\sim 6\%$ found for Mode-I (Park & Ricotti 2012) to a 100% duty cycle where the accreting BH is always "on".

Figure 7 shows the time-averaged density (top), temperature (middle), and radial velocity (bottom) profiles as a function of radius for $M_{\text{BH}} = 10^6 M_{\odot}$ (run M6N1) with different bulge masses $M_{\text{bulge}} = 10^7, 10^8$, and $10^9 M_{\odot}$ (i.e., $\delta_{\text{bulge-BH}} = 10^1, 10^2$, and 10^3). The density inside the Strömgren radius increases linearly with increasing M_{bulge} whereas the temperature profile only shows a minor change of slope. The slope of the temperature profile becomes flatter due to the enhanced density with increasing $\delta_{\text{bulge-BH}}$ returning a consistent result with previous works [e.g., see Figure 8 of Park & Ricotti (2011)]. The vertical dashed lines indicate the average location of the ionization front (i.e., Strömgren radius). The radial velocity profiles also show differences.

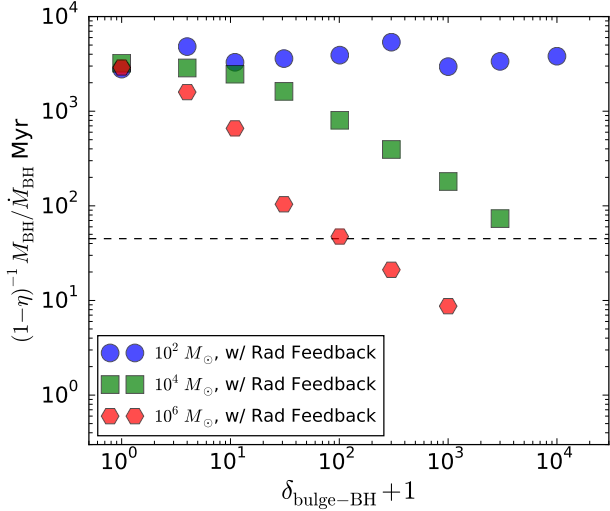


FIG. 9.— Timescales for BH masses $M_{\text{BH}} = 10^2$ (circles), 10^4 (squares), and $10^6 M_{\odot}$ (hexagons) to double the initial mass as a function of $\delta_{\text{bulge-BH}}$. Salpeter (or e -folding) timescale for $\eta = 0.1$ accreting at Eddington rate is shown as a dashed line.

In general, the magnitude of the radial velocity increases as a function of M_{bulge} . For $M_{\text{bulge}} = 10^7 M_{\odot}$, outflows are clearly seen in the outer part of the Strömgen sphere (shown as a dotted line), indicating that the oscillatory accretion rate due to the gas depletion inside the Strömgen sphere is still occurring. However, the outflow weakens with increasing M_{bulge} , leading to a steady accretion rate. Similar to the case without radiation feedback the increase of the accretion rate is dominated by the increase in the gas density near the Bondi radius of the BH. The oscillations instead appear to cease when $r_{\text{B,eff}}$ becomes larger than the Strömgen radius.

Figure 8 shows accretion rates normalized by the Bondi rate for $100 M_{\odot}$ BHs (runs M2N5, circles), $10^4 M_{\odot}$ BHs (runs M4N3, squares), and $10^6 M_{\odot}$ BHs (runs M6N1, hexagons). The overall accretion rate when radiation feedback is included is about 1 percent of the Bondi rate, but the dependence on M_{bulge} is similar to the case without radiation feedback (see Figure 5). Due to the increased effective accretion radius when $M_{\text{bulge}} \gtrsim M_{\text{bulge,crit}}$, the accretion rate increases as $\dot{M}_{\text{BH}} \propto M_{\text{bulge}}/M_{\text{bulge,crit}}$ (shown as a solid line). For $10^6 M_{\odot}$ BHs (runs M6N1), the accretion rate increases as approximately M_{bulge} for $M_{\text{bulge}} \gtrsim 10^6 M_{\odot}$, but again at a rate of 1% compared to the simulations without radiative feedback. At $M_{\text{bulge}} \sim 10^7 M_{\odot}$ the oscillations are still present, but for $M_{\text{bulge}} \sim 10^8 M_{\odot}$ the accretion rate becomes steady and approaches $\dot{M}_{\text{B}} \sim \dot{M}_{\text{Edd}}$ and goes beyond the Eddington rate at $M_{\text{bulge}} \sim 10^9 M_{\odot}$. This suggests a possibility of the hyper-Eddington accretion regime, however this work does not establish an upper limit on such high accretion rates (e.g., Inayoshi et al. 2015a). For the runs with smaller mass BHs (runs M4N3) the same trend of the accretion rate $\dot{M}_{\text{BH}} \propto M_{\text{bulge}}/M_{\text{bulge,crit}}$ is found. However, probably due to the sharper transition of $r_{\text{B,eff}}$ from r_{B} to $\delta_{\text{bulge-BH}} r_{\text{B}}$ as $\delta_{\text{bulge-BH}}$ is increased, the oscillations are damped closer to $M_{\text{bulge}} \sim 10^7 M_{\odot}$.

Figure 9 shows the timescales for BH masses with $M_{\text{BH}} = 10^2, 10^4,$ and $10^6 M_{\odot}$ to double the initial mass as a function of $\delta_{\text{bulge-BH}}$. The horizontal line shows the Salpeter

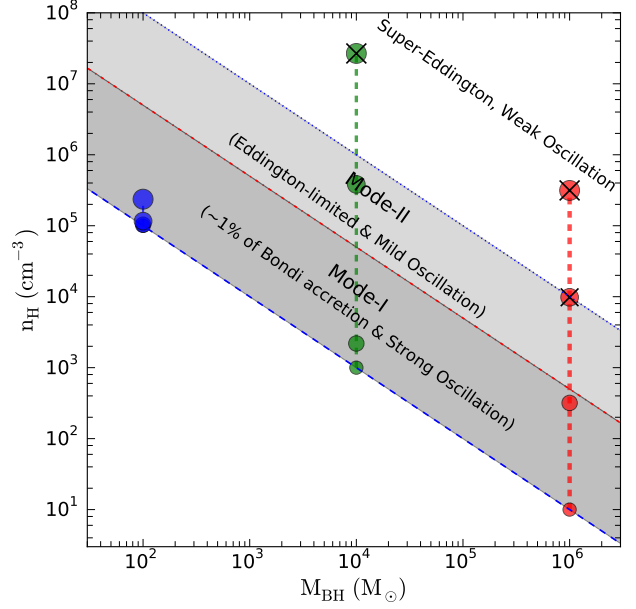


FIG. 10.— Accretion regimes as a function of M_{BH} and $n_{\text{H},\infty}$. Symbols show the shift of accretion regime (from bottom to top) due to the enhanced density as a function of $\delta_{\text{bulge-BH}}$ for BH masses $10^2, 10^4,$ and $10^6 M_{\odot}$. For each BH mass, symbols with different sizes show $\delta_{\text{bulge-BH}} = 0, 10^1, 10^2,$ and 10^3 from bottom to top. Symbols marked with crosses indicate non-oscillatory cases.

(1964) (or e -folding) timescale when $\eta = 0.1$ and $L = L_{\text{Edd}}$ are assumed. For a BH mass $M_{\text{BH}} = 10^2 M_{\odot}$, the accretion timescale is ~ 3 Gyr with no apparent dependence on $\delta_{\text{bulge-BH}}$. On the other hand, the accretion timescale for $M_{\text{BH}} = 10^6 M_{\odot}$ is inversely proportional to the bulge mass as $M_{\text{BH}}/\dot{M}_{\text{BH}} \propto (\delta_{\text{bulge-BH}} + 1)^{-1}$. At $\delta_{\text{bulge-BH}} \sim 10^2$, the accretion timescale for $M_{\text{BH}} = 10^6 M_{\odot}$ is similar to the Salpeter timescale. For a BH mass $M_{\text{BH}} = 10^4 M_{\odot}$, the accretion timescale does not show a dependence on $\delta_{\text{bulge-BH}}$ for $\delta_{\text{bulge-BH}} \lesssim 10^2$ while it decreases with increasing $\delta_{\text{bulge-BH}}$ with the similar slope for $10^6 M_{\odot}$.

4. DISCUSSION AND SUMMARY

Accretion regimes as a function of M_{BH} and $n_{\text{H},\infty}$ explained in Figure 1 can be consolidated in presence of the bulge for various BH masses. In Figure 10, the symbols show the transitions between accretion regimes (from bottom to top) due to the enhanced density as a function of $\delta_{\text{bulge-BH}}$ for BH masses $10^2, 10^4,$ and $10^6 M_{\odot}$. For each BH mass, symbols with different sizes show $\delta_{\text{bulge-BH}} = 0, 10^1, 10^2,$ and 10^3 from bottom to top. Note that for $M_{\text{BH}} = 10^6 M_{\odot}$, the density increases linearly with $\delta_{\text{bulge-BH}}$, however the density does not increase for $M_{\text{BH}} = 10^2 M_{\odot}$ because $M_{\text{bulge}} < M_{\text{bulge,crit}} \sim 10^6 M_{\odot}$ in this case ($T_{\infty} = 10^4$ K). Symbols with crosses in Figure 10 indicate simulations which do not show oscillations.

Although the accretion regime as a function of M_{BH} and $n_{\text{H},\infty}$ in Figure 10 is successful in explaining the transition of the accretion rates and overall oscillatory behavior presented in this work, however, the relative location of the Strömgen radius and effective Bondi radius also affects the oscillatory behavior of the accretion. For example, a simulation with $M_{\text{BH}} = 10^6 M_{\odot}$, $n_{\text{H},\infty} = 10^{-2} \text{ cm}^{-3}$, and

$\delta_{\text{bulge-BH}} = 10^3$ where the effective gas density is enhanced to 10 cm^{-3} does not show the same oscillatory behavior as the one with $M_{\text{BH}} = 10^6 M_{\odot}$, $n_{\text{H},\infty} = 10 \text{ cm}^{-3}$ without a bulge. This is due to the same argument explained in section 3.2 related to Figure 7 that $r_{\text{B,eff}}$ should be smaller than the average Strömgen radius for simulations to be oscillatory.

We have focused on accretion from a cold neutral gas reservoir, which might be the dominant medium in the first galaxies that form in the early universe. However, accretion onto SMBHs in evolved galaxies is far more complicated since the gas is multi-phase with a hot and a cold component, likely produced by the star formation and the feedback from the SMBH itself.

This is clearly a first step in understanding the role of the galactic environment in feeding a seed BH at the center of a galaxy: we have assumed accretion from a uniform density medium and neglected angular momentum of the gas that is clearly important for accretion from the disk in a disk galaxy but is also likely important in elliptical and spheroidal galaxies (Ciotti & Ostriker 2007; Ciotti et al. 2009; Novak et al. 2011). In future work, the growth of seed BHs embedded in various bulge sizes will be studied in realistic cosmological simulations, guided by findings of these idealized simulations.

In this paper, we explore the role of bulge component in radiation-regulated accretion onto seed IMBHs accreting from cold and hot medium at the center of primordial galaxies in the early universe. Here we list our main findings.

- The presence of a massive bulge makes the effective Bondi radius $r_{\text{B,eff}}$ increase approximately to $r_{\text{B,eff}} \simeq r_{\text{B}} M_{\text{bulge}}/M_{\text{BH}}$ for $M_{\text{bulge}} > M_{\text{bulge,crit}}$ while for $M_{\text{bulge}} < M_{\text{bulge,crit}}$ the bulge has no effect on the accretion radius and the BH growth.
- Without radiative feedback, the accretion rate onto the central BH increases as $\dot{M}_{\text{BH}} = \dot{M}_{\text{B}} M_{\text{bulge}}/M_{\text{bulge,crit}}$ when $M_{\text{bulge}} > M_{\text{bulge,crit}}$. This is due to the bulge gravitational potential force-feeding the BH and enhancing the density of gas near the Bondi radius by a factor $M_{\text{bulge}}/M_{\text{bulge,crit}}$.
- Including radiative feedback suppresses the accretion rate to 1 percent of the Bondi rate, however a similar dependence of the accretion rate on the bulge mass $\dot{M}_{\text{BH}} \sim 1\% \dot{M}_{\text{B}} M_{\text{bulge}}/M_{\text{bulge,crit}}$ is found for $M_{\text{bulge}} > M_{\text{bulge,crit}}$. The increased gas density near the Bondi radius due to fueling from the bulge gravitational potential affects the periodic behavior of the accretion rate that eventually becomes steady for bulge masses between a few to 10 times $M_{\text{bulge,crit}}$.
- For accretion from a cold gas reservoir, a minimum bulge mass ($M_{\text{bulge}} \sim 10^6 M_{\odot}$) exists, above which the effective Bondi radius is $r_{\text{B,eff}}/r_{\text{B}} \gtrsim 1$, which is a necessary condition to boost the BH fueling rate. This might help understanding the low luminosity for the BHs in small systems such as globular clusters or dwarf galaxies. For such systems, the radiative feedback is effective in suppressing the accretion rate to 1 percent of the Bondi rate.
- For the high mass end of IMBHs, BHs grow fast when $\delta_{\text{bulge-BH}} \gtrsim 1$ meaning that the early development of $M_{\text{BH}} - \sigma$ relationship might be a natural consequence of radiation-regulated BH accretion at the centers of galaxies along with the building of stellar bulge mass profile.
- For the low mass end of IMBHs ($M_{\text{BH}} \sim 10^2 M_{\odot}$), BHs are harder to grow since the accretion rate is close to 1 percent of Bondi rate for $\delta_{\text{bulge-BH}} < \delta_{\text{crit}} \sim 10^4$. Thus, assuming that the hosts of these small seed BHs have initially $\delta_{\text{bulge-BH}} < 10^4$ ($M_{\text{bulge}} < 10^6 M_{\odot}$), the growth timescale for low mass IMBHs suggests that light seed BHs, such as Population III remnants, are not able to grow coevally with the bulge. On the other hand, heavy BHs ($M_{\text{BH}} \gtrsim 10^5 M_{\odot}$) from direct collapse can grow efficiently together with the bulge as long as $\delta_{\text{bulge-BH}} \gtrsim 1 - 10$. This result has similar implications about the fate of *light* and *heavy* seed BHs, as the finding of Volonteri & Natarajan (2009) obtained in models where the $M_{\text{BH}} - \sigma$ relation is driven by major mergers.

In conclusion, for systems with the bulge masses larger than critical ($\sim 10^6 M_{\odot}$) the central BH transitions into a new accretion regime in which both the accretion rate and duty cycle are maximized despite the presence of radiative feedback. In this regime, the accretion rate onto the BH reaches and goes beyond the Eddington rate. While this signals an exciting possibility of reaching the hyper-Eddington accretion regime, the current work does not establish an upper limit on such high accretion rates, a topic which will be explored in future work.

This work is supported by the National Science Foundation under the Theoretical and Computational Astrophysics Network (TCAN) grants AST-1332858, AST-1333360, AST-1333514. T.B. acknowledges the support from the Alfred P. Sloan Foundation under Grant No. BR2013-016.

REFERENCES

- Abel, T., Bryan, G. L., & Norman, M. L. 2000, ApJ, 540, 39
 Alexander, T., & Natarajan, P. 2014, Science, 345, 1330
 Alvarez, M. A., Wise, J. H., & Abel, T. 2009, ApJ, 701, L133
 Aykatalp, A., Wise, J. H., Spaans, M., & Meijerink, R. 2014, ApJ, 797, 139
 Baldassare, V. F., Reines, A. E., Gallo, E., & Greene, J. E. 2015, ApJ, 809, L14
 Begelman, M. C. 1979, MNRAS, 187, 237
 Begelman, M. C., Volonteri, M., & Rees, M. J. 2006, MNRAS, 370, 289
 Bondi, H. 1952, MNRAS, 112, 195
 Bondi, H., & Hoyle, F. 1944, MNRAS, 104, 273
 Bromm, V., Coppi, P. S., & Larson, R. B. 1999, ApJ, 527, L5
 Carr, B. J., Bond, J. R., & Arnett, W. D. 1984, ApJ, 277, 445
 Choi, J.-H., Shlosman, I., & Begelman, M. C. 2013, ApJ, 774, 149
 Ciotti, L., & Ostriker, J. P. 2007, ApJ, 665, 1038
 Ciotti, L., Ostriker, J. P., & Proga, D. 2009, ApJ, 699, 89
 Davies, M. B., Miller, M. C., & Bellovary, J. M. 2011, ApJ, 740, L42
 Devecchi, B., & Volonteri, M. 2009, ApJ, 694, 302
 Dwek, E., et al. 1995, ApJ, 445, 716
 Fan, X., et al. 2001, AJ, 122, 2833
 —. 2003, AJ, 125, 1649
 —. 2006, AJ, 132, 117
 Ferrarese, L., & Merritt, D. 2000, ApJ, 539, L9
 Fryer, C. L., Woosley, S. E., & Heger, A. 2001, ApJ, 550, 372
 Greene, J. E., & Ho, L. C. 2004, ApJ, 610, 722
 Haehnelt, M. G., Natarajan, P., & Rees, M. J. 1998, MNRAS, 300, 817
 Hayes, J. C., Norman, M. L., Fiedler, R. A., Bordner, J. O., Li, P. S., Clark, S. E., ud-Doula, A., & Mac Low, M.-M. 2006, ApJS, 165, 188
 Hernquist, L. 1990, ApJ, 356, 359
 Inayoshi, K., Haiman, Z., & Ostriker, J. P. 2015a, arXiv:1511.02116
 Inayoshi, K., Visbal, E., & Kashiyama, K. 2015b, MNRAS, 453, 1692

- Jeon, M., Pawlik, A. H., Greif, T. H., Glover, S. C. O., Bromm, V., Milosavljević, M., & Klessen, R. S. 2012, *ApJ*, 754, 34
- Jiang, Y.-F., Stone, J. M., & Davis, S. W. 2014, *ApJ*, 796, 106
- Johnson, J. L., Whalen, D. J., Fryer, C. L., & Li, H. 2012, *ApJ*, 750, 66
- Kafle, P. R., Sharma, S., Lewis, G. F., & Bland-Hawthorn, J. 2014, *ApJ*, 794, 59
- Katz, H., Sijacki, D., & Haehnelt, M. G. 2015, *MNRAS*, 451, 2352
- King, A. 2003, *ApJ*, 596, L27
- Krolik, J. H. 2004, *ApJ*, 615, 383
- Li, Y. 2011, arXiv:1109.3442
- Lodato, G., & Natarajan, P. 2006, *MNRAS*, 371, 1813
- Mack, K. J., Ostriker, J. P., & Ricotti, M. 2007, *ApJ*, 665, 1277
- MacLeod, M., Trenti, M., & Ramirez-Ruiz, E. 2015, arXiv:1508.07000
- Madau, P., & Rees, M. J. 2001, *ApJ*, 551, L27
- Magorrian, J., et al. 1998, *AJ*, 115, 2285
- Mayer, L., Fiacconi, D., Bonoli, S., Quinn, T., Roškar, R., Shen, S., & Wadsley, J. 2015, *ApJ*, 810, 51
- McKee, C. F., & Ostriker, J. P. 1977, *ApJ*, 218, 148
- Miller, M. C., Farrell, S. A., & Maccarone, T. J. 2014, *ApJ*, 788, 116
- Milosavljević, M., Couch, S. M., & Bromm, V. 2009, *ApJ*, 696, L146
- Mortlock, D. J., et al. 2011, *Nature*, 474, 616
- Murray, N., Quataert, E., & Thompson, T. A. 2005, *ApJ*, 618, 569
- Natarajan, P. 2011, *Bulletin of the Astronomical Society of India*, 39, 145
- Natarajan, P., & Treister, E. 2009, *MNRAS*, 393, 838
- Novak, G. S., Ostriker, J. P., & Ciotti, L. 2011, *ApJ*, 737, 26
- Ohsuga, K., & Mineshige, S. 2011, *ApJ*, 736, 2
- Omukai, K., Schneider, R., & Haiman, Z. 2008, *ApJ*, 686, 801
- Ostriker, J. P., Choi, E., Ciotti, L., Novak, G. S., & Proga, D. 2010, *ApJ*, 722, 642
- Pacucci, F., Volonteri, M., & Ferrara, A. 2015, *MNRAS*, 452, 1922
- Park, K., & Ricotti, M. 2011, *ApJ*, 739, 2
- . 2012, *ApJ*, 747, 9
- . 2013, *ApJ*, 767, 163
- Park, K., Ricotti, M., Di Matteo, T., & Reynolds, C. S. 2014a, *MNRAS*, 437, 2856
- . 2014b, *MNRAS*, 445, 2325
- Pelupessy, F. I., Di Matteo, T., & Ciardi, B. 2007, *ApJ*, 665, 107
- Reines, A. E., Greene, J. E., & Geha, M. 2013, *ApJ*, 775, 116
- Reines, A. E., Sivakoff, G. R., Johnson, K. E., & Brogan, C. L. 2011, *Nature*, 470, 66
- Ricotti, M. 2009, *MNRAS*, 392, L45
- Ricotti, M., Gnedin, N. Y., & Shull, J. M. 2001, *ApJ*, 560, 580
- Ricotti, M., & Ostriker, J. P. 2004, *MNRAS*, 352, 547
- Salpeter, E. E. 1964, *ApJ*, 140, 796
- Silk, J., & Rees, M. J. 1998, *A&A*, 331, L1
- Springel, V., Di Matteo, T., & Hernquist, L. 2005, *MNRAS*, 361, 776
- Springel, V., & Hernquist, L. 2003, *MNRAS*, 339, 289
- Stone, J. M., & Norman, M. L. 1992, *ApJS*, 80, 753
- Strohmayer, T. E., & Mushotzky, R. F. 2009, *ApJ*, 703, 1386
- Tremaine, S., et al. 2002, *ApJ*, 574, 740
- Volonteri, M. 2012, *Science*, 337, 544
- Volonteri, M., Haardt, F., & Madau, P. 2003, *ApJ*, 582, 559
- Volonteri, M., & Natarajan, P. 2009, *MNRAS*, 400, 1911
- Volonteri, M., & Rees, M. J. 2005, *ApJ*, 633, 624
- Widrow, L. M., & Dubinski, J. 2005, *ApJ*, 631, 838
- Willott, C. J., McLure, R. J., & Jarvis, M. J. 2003, *ApJ*, 587, L15
- Willott, C. J., et al. 2010, *AJ*, 139, 906
- Wu, X.-B., et al. 2015, *Nature*, 518, 512
- Yoo, J., & Miralda-Escudé, J. 2004, *ApJ*, 614, L25
- Yue, B., Ferrara, A., Salvaterra, R., Xu, Y., & Chen, X. 2014, *MNRAS*, 440, 1263